A New Zero Voltage Switching Bidirectional DC-DC Converter with Simple Structure

Mahmood Vesali[1†], **Marzieh Khorami**[2], and **Farhad Ghafoorian**[1], Non-members

ABSTRACT

A new zero voltage switching bidirectional DC-DC converter proposes in this paper. In the proposed converter, without adding any auxiliary switches and with a simple snubber, soft switching conditions are created, which simplifies the structure of the converter. The control of the switches in the proposed converter is complementary to each other, so the control circuit of the converter is simple and does not need any extra control circuit. The coupled inductors used in the converter, in addition to controlling the resonant inductor energy, transfer circulating currents to the input or output, which reduces the loss energy in the converter and increases the efficiency. The proposed converter is fully analyzed, and to verify the theoretical analysis, a 300-watt prototype of the converter is implemented and tested, resulting in an efficiency of about 95.5% at full load.

Keywords: Bidirectional converters, Zero voltage switching (ZVS), Efficiency

1. INTRODUCTION

Nowadays, bidirectional converters are widely used in industry. These converters are used as controllers to store energy [1], [2]. These converters are widely used in photovoltaic systems [3–6], electric vehicle systems [7-9], wind energy systems [10–13], and fuel cell systems [14–16]. In these systems, batteries and supercapacitors are used to store energy, and the bidirectional converter controls the transfer of power between the storage elements and the main system. In all the systems mentioned, this process is used to receive power and store it when the system power is high. and delivering power to the system through storage elements when the main power is reduced. Since efficiency is important in the above systems, the placement of converters reduces the efficiency of the system. Therefore, the higher the efficiency of the bidirectional converter, the less effect it has on the efficiency of the whole system. Therefore, in recent years, high-efficiency converters have become particularly important [17–19]. Hard-switching converters have such low efficiencies that soft-switching techniques have been proposed to increase efficiency. These techniques minimize voltage and current overlap during switching, which reduces switching losses and increases efficiency. Commonly used techniques are resonant [20], [21], zero voltage switching (ZVS) [22–24], zero current switching (ZCS) [25], [26], and zero voltage zero current switching (ZVZCS) [27]. In the resonant converter, by creating a resonant on the voltage and current of the switch, the rising rate of the voltage and current is decreased and soft switching is provided, but this technique creates a high current stress on the switch. Therefore, these converters are not suitable for use in high-power systems.

In [20] and [21], two resonant converters are proposed, and these converters have high current stress. Also, these converters have many elements, which increases volume and cost. Zero-voltage switching is one technique to decrease switching losses and increase efficiency; in [22], a new converter with this technique is introduced. In this converter, high voltage gain and full ZVS are achieved, but due to the high number of elements, this converter has a high volume and cost. Also, in this converter, eight switches are used, and the control of these switches is very complex. In [23], a new ZVS bidirectional converter is proposed. This converter has an interleaved structure that increases the reliability of the converter, but this structure has high complexity with eight switches, which increases conduction losses and decreases efficiency. In this converter, the control of these eight switches is very difficult. A high-voltage gain ZVS bidirectional converter is presented in [24]. Although this converter has a high voltage gain and efficiency, its complex structure makes it difficult to implement. Also, the control of the switches in this converter is very complex, so the design and implementation of the control circuit are difficult. Zero-current switching is another technique to establish soft switching and decrease switching losses. [25] and [26] are two references that introduce this technique. [25] has a high efficiency but a high number of elements, which have complex structures. [26] has a simple structure with high efficiency, but in this converter, due to the nature of the auxiliary circuit, the current stress on the elements is high. The converter also has a special tuning on the switches, which have a complex control circuit. Some references have used both soft switching techniques,

Manuscript received on October 26, 2022; revised on February 19, 2023; accepted on February 23, 2023. This paper was recommended by Associate Editor Matheepot Phattanasak.

[1]The authors is with Department of Electrical Engineering, Isfahan (khorasgan) Branch, Islamic Azad University, Isfahan, Iran,

[2]The author is with Department of Computer Engineering, Isfahan (khorasgan) Branch, Islamic Azad University, Isfahan, Iran ,

[†]Corresponding author: mahmoodvesali645@gmail.com

Digital Object Identifier: 10.37936/ecti-eec.2023212.249829

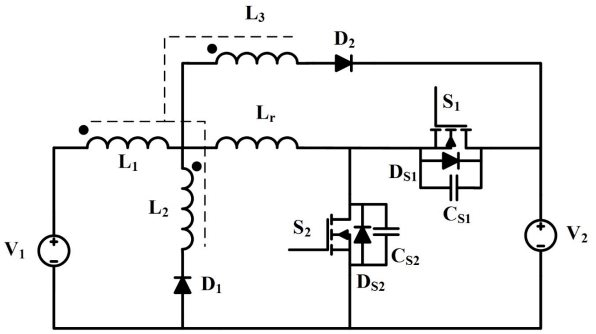

Fig. 1: Structure of the proposed converter.

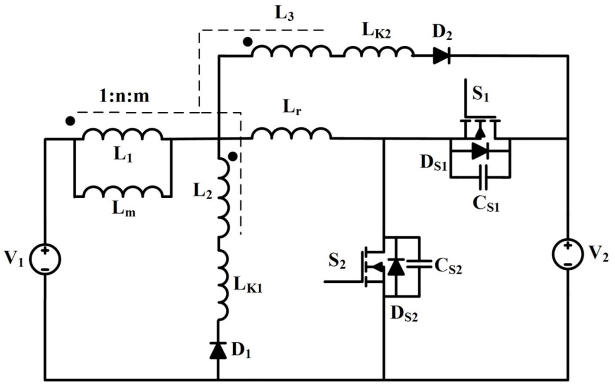

Fig. 2: Equivalent of the proposed converter.

which are described in a sample of this converter in [27]. This converter has a low number of elements and a simple structure with high efficiency, but it also has four switches with special tuning and a complex control circuit. Also, current stresses on the switches are high.

In this paper a new ZVS bidirectional DC-DC converter is proposed that has high efficiency. The proposed converter has a simple structure without any extra switches. By using only one snubber circuit, the ZVS condition is provided for both directions, and with coupled inductors, circulating currents are controlled. The proposed converter is analyzed in Section 2, and in Section 3, the design of the converter elements and important relationships are given. The experimental results of the proposed converter are presented in Section 4; in Section 5, a comparison of the proposed converter with other converters is given, and finally, the conclusion of the paper is presented in Section 6.

2. THE PROPOSED CONVERTER STRUCTURE AND ANALYSIS

The proposed converter is shown in Fig. 1. The converter consists of three inductors coupled to one core. The proposed converter does not have any auxiliary switches. D_1 and D_2 are placed to control current flow on coupled inductors, which, according to the switching mode of the converter and the on and off times of these diodes, transfer the energy of the coupled inductors as well as their leakage inductors to the input or output of the converter. The equivalent circuit of the proposed converter with coupled inductors is shown in Fig. 2. As can be seen, the coupled inductors include a magnetic inductor and leakage inductors. The converter is fully analyzed in both modes.

2.1 Boost Mode

In boost mode, the power is transferred from V_1 to V_2. In this mode, S_2 is the main switch, and S_1 is an auxiliary switch that is switched as a complement to S_2. There are eight intervals in boost mode, which is described below. The key waveforms of the proposed converter in boost mode are shown in Fig. 3.

Interval 1 ($t_0 - t_1$): This interval begins when $S_2$is

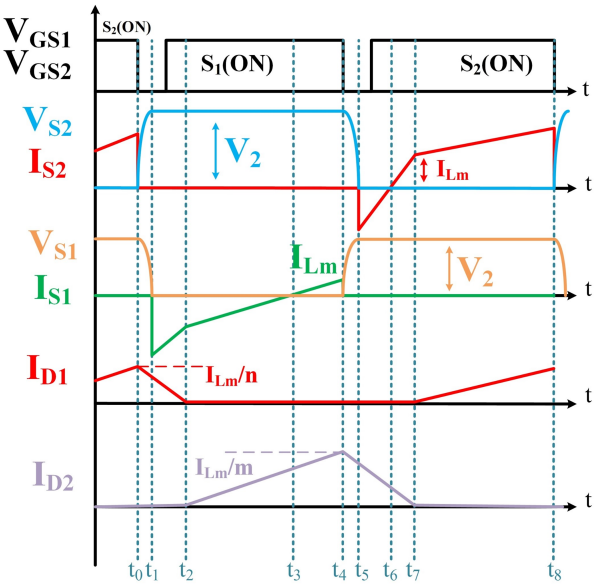

Fig. 3: Key waveforms of the proposed converter in boost mode.

turned off. Since L_r current cannot change immediately, a resonance occurred between L_r, C_{s1} and C_{s2}. This resonance causes to discharge C_{s1} and charge C_{s2}. The equations for these charges and discharges are shown below.

$$i_{CS1} = \frac{V_2}{Z} sin\omega_r \left(t - t_0\right) \tag{1}$$

$$V_{CS1} = V_{S1} = V_2 cos\omega_r \left(t - t_0\right) - V_2 \tag{2}$$

$$Z = \sqrt{\frac{L_r}{C_{S1}}} \tag{3}$$

$$\omega_r = \frac{1}{\sqrt{L_r \left(C_{S1} + C_{S2}\right)}} \tag{4}$$

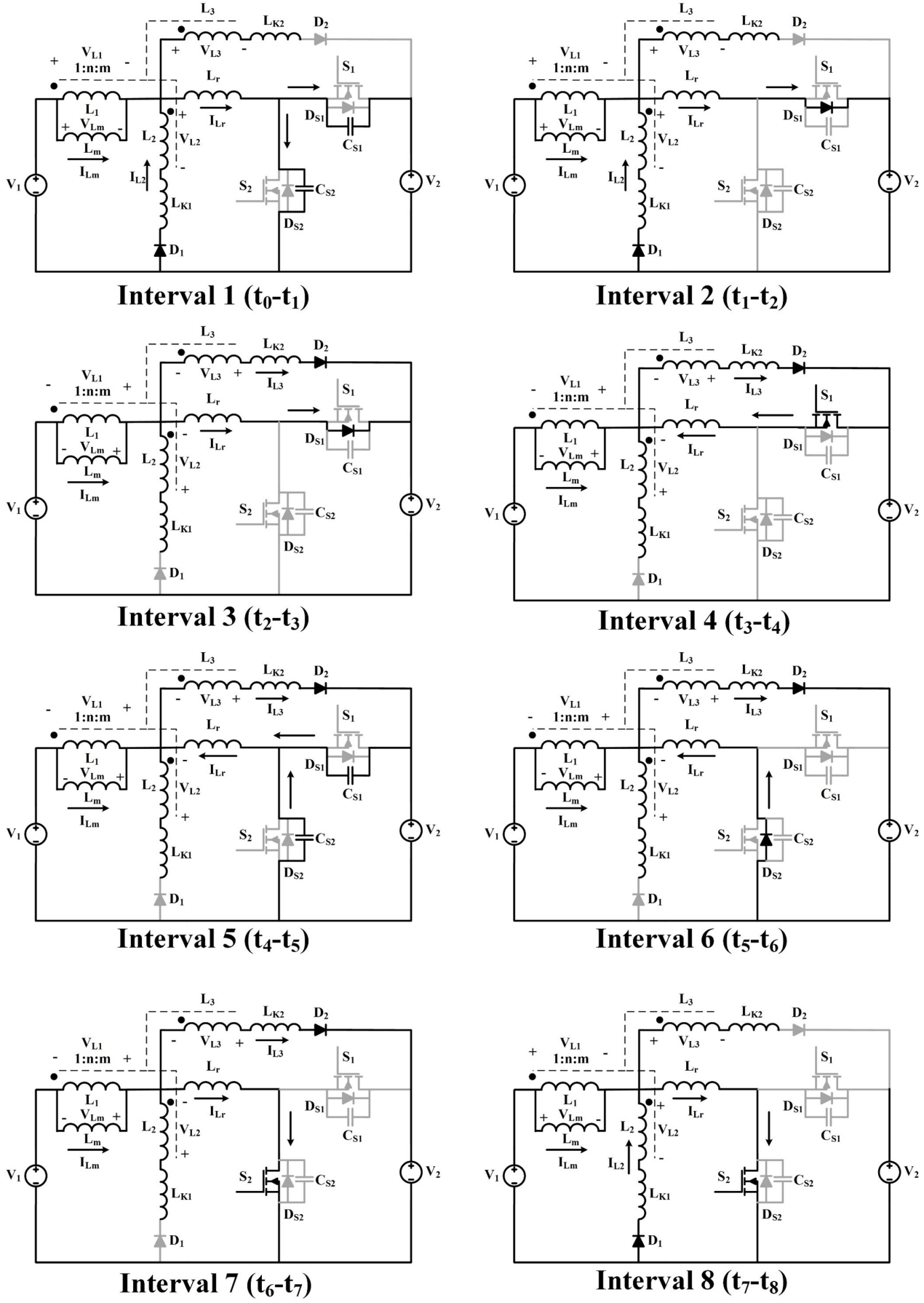

***Fig. 4**: Equivalent circuit of the proposed converter in boost mode.*

Interval 2 ($t_1 - t_2$): When C_{S1} is fully discharged and the body diode of S_1 conducts, this interval begins. Due to the conductivity of the body diode, the voltage of the switch is at zero, and if the switch is turned on, it is turned on under the zero voltage condition. Therefore, S_1 is turned on under the ZVS condition for the duration of this interval.

Interval 3 ($t_2 - t_3$): In this interval, the direction of L_1 current is changed, so D_1 turns off and D_2 turns on. But in this interval, L_r current does not change direction.

Interval 4 ($t_3 - t_4$): In this interval, the current of L_r reaches zero and changes direction. Therefore, the current from S_1transferred from the body diode to the switch. This condition continues until S_1 is turned off.

Interval 5 ($t_4 - t_5$): This interval begins when S_1 is turned off. Due to the direction of $L_r$current and the fact that inductor current cannot change suddenly, a resonance occurs between L_r, C_{S1}, and C_{S2}. This resonance causes C_{S1} to be charged and C_{S2} to be discharged, so S_1 is turned off under the ZVS condition. The equation of this resonant is shown below.

$$i_{CS2} = \frac{V_2}{Z} sin\omega_r \left(t - t_4\right) \tag{5}$$

$$V_{CS2} = V_{S2} = V_2 cos\omega_r \left(t - t_4\right) - V_2 \tag{6}$$

$$Z = \sqrt{\frac{L_r}{C_{S2}}} \tag{7}$$

$$\omega_r = \frac{1}{\sqrt{L_r \left(C_{S1} + C_{S2}\right)}} \tag{8}$$

Interval 6 ($t_5 - t_6$): With full discharge of C_{S2}, the body diode of this switch conducts and the voltage of the switch is clamped to zero. Therefore, the ZVS condition is established for this switch.

Interval 7 ($t_6 - t_7$): In this interval, the current of reaches zero and the direction of this current is changed, so the current of S_2 is transferred from the body diode to the switch. During intervals 6 and 7, the current of the switch rises with a slope as shown below.

$$\frac{V_{1-V_{Lm}}}{L_r} \tag{9}$$

Interval 8 ($t_7 - t_8$): When the current of the switch reaches I_{Lm}, the converter act as a boost converter when the switch is on and the main inductor is charged. In this interval, because of the direction of L_1 current, D_2 turns off and D_1 turns on. This interval ends when S_2 is turned off and the converter returns to interval 1.

The equivalent of these 8 intervals is shown in Fig. 4.

2.2 Buck Mode

The converter in buck mode has eight intervals at one switching cycle. Before starting interval 1, S_1 is on and the current is transmitted to the output. According to the polarity created on L_m, D_1 is off and D_2 is on. With this condition, interval 1 starts. The key waveforms of the converter in buck mode are shown in Fig. 5.

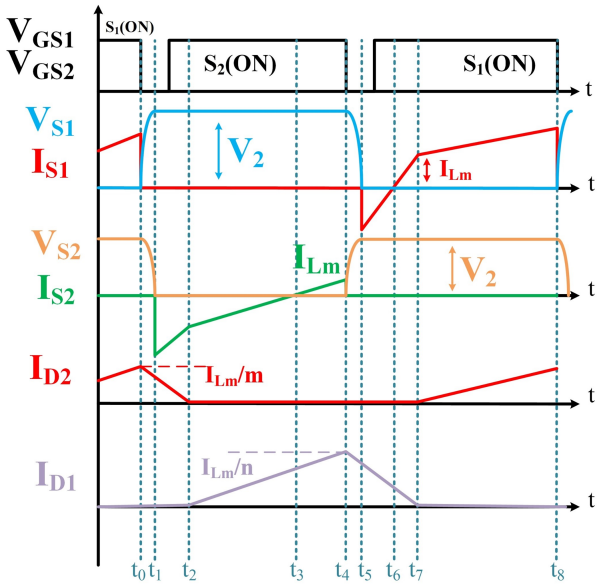

***Fig. 5**: Key waveform of the proposed converter in buck mode.*

Interval 1 ($t_0 - t_1$): When S_1 is turned off due to the direction of L_r current, C_{S1} is charged and C_{S2} is discharged. These charges and discharges are resonant, and the equations of this resonant are similar to interval 1 in boost mode.

Interval 2 ($t_1 - t_2$): When C_{S2} is fully discharged, the body diode of this switch conducts, and the ZVS condition is provided for the switch. In this interval, the switch's current is raised linearly with a slope, as shown below.

Interval 6 ($t_5 - t_6$): By full discharge of C_{S1}, the body diode of this switch conducts, and the ZVS condition is established for this switch. At this interval, S1 is turned on under the ZVS condition.

Interval 7 ($t_6 - t_7$): When the current of L_r reaches to zero, the current direction of S_1 is changed and is transferred from the body diode to the switch.

Interval 8 ($t_7 - t_8$): In this interval, the current of L_r and also the current of S_1 reach to I_{Lm}, therefore, the converter acts as the conventional buck converter when the main switch is on and the main inductor is charged. When the switch is turned off, this interval ends and the switching cycle also ends.

The equivalent of these 8 intervals is shown in Fig. 6.

$$\frac{V_1 + V_2}{L_r} \tag{10}$$

Interval 3 ($t_2 - t_3$): In this interval, the direction of L_1 current is changed, which causes D_2 to be turned off and D_1 to be turned on. So, the slope of the current has changed, as shown below.

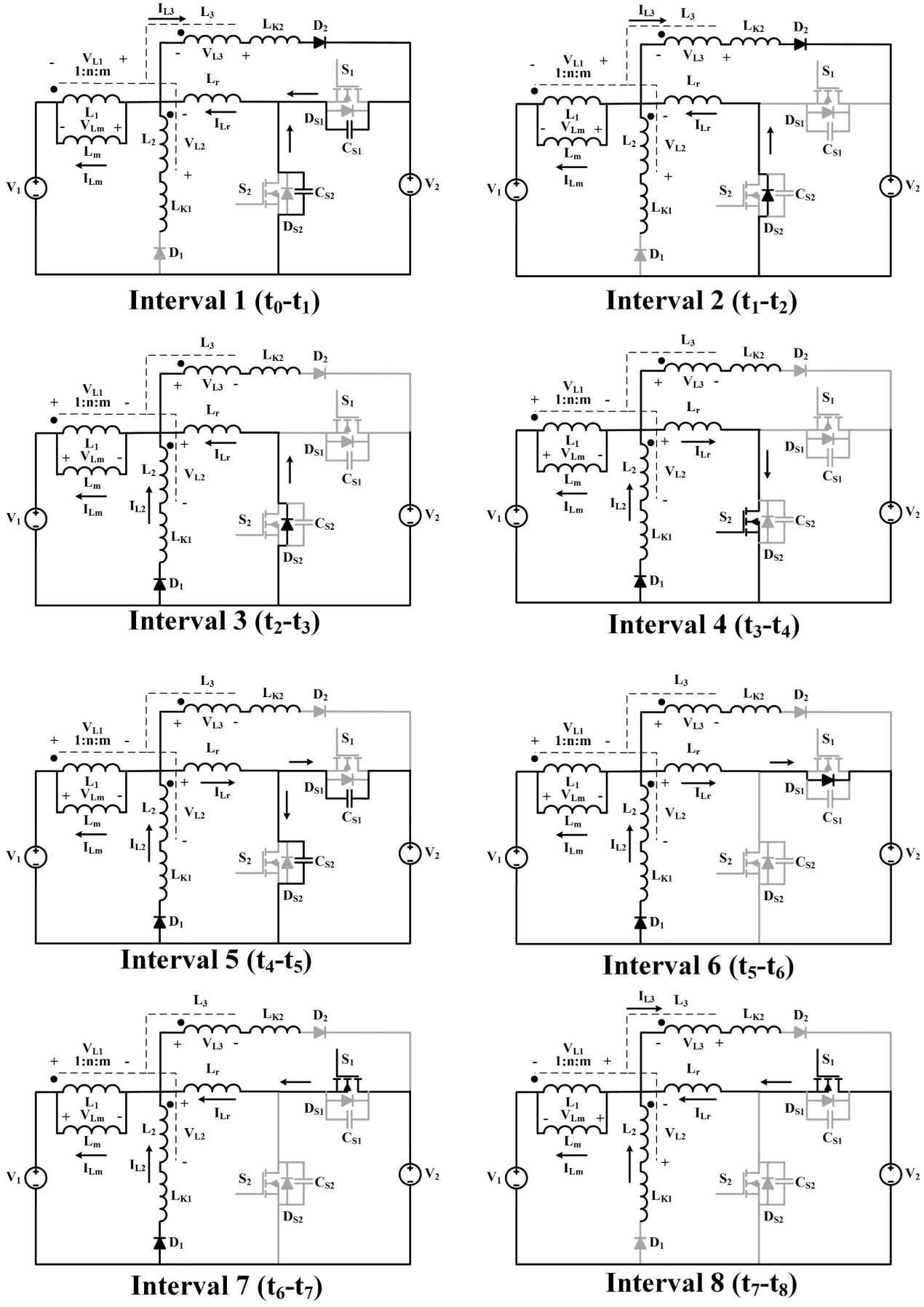

***Fig. 6**: Equivalent circuit of the proposed converter in buck mode.*

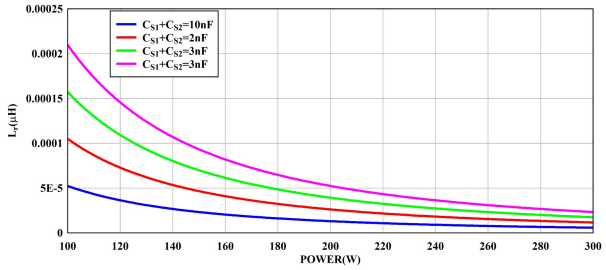

***Fig. 7**: L_r versus power and C_S.*

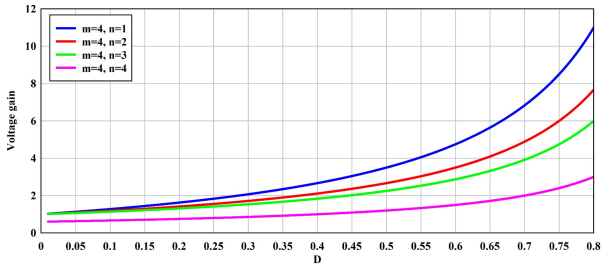

***Fig. 8**: Voltage gain in boost mode with fixed value of m and various value of n.*

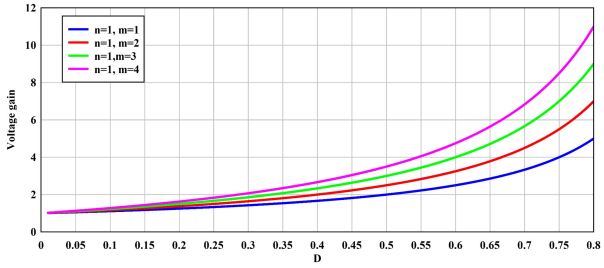

***Fig. 9**: Voltage gain in boost mode with fixed value of n and various value of m.*

$$\frac{nV_{Lm}}{L_r} \tag{11}$$

Interval 4 (t_3−t_4): This interval starts when the current of L_r reaches zero and changes direction; therefore, the current of S_2 is transferred from the body diode to the switch.

Interval 5 ($t_4 - t_5$): S_2 is turned off in this interval. Since the current of L_r is continued, this current cause to charge C_{S2} and discharge C_{S1}. These charge and discharge are resonantly.

3. DESIGN OF ELEMENTS

3.1 Design and Calculations of L_r

To design L_r, the inductor energy, which must completely discharge the snubber capacitors, is important. Therefore, the energy equation in these elements helps to design the inductor.

$$\frac{1}{2}L_r I^2 > \frac{1}{2}C_S V^2 \tag{12}$$

According to the proposed converter structure, the current of L_r is equal to I_{Lm} and the voltage of snubber capacitors is equal to V_2.

$$\frac{1}{2}L_r I_{Lm}^2 > \frac{1}{2}\left(C_{S1} + C_{S2}\right)V_2^2 \tag{13}$$

$$L_r > \frac{\left(C_{S1} + C_{S2}\right)V_2^2}{I_{Lm}^2} \tag{14}$$

According to Eq. (14), the curves of Fig. 7 have been drawn, which can be useful in selecting the inductor according to the snubber capacitors. To get the right amount of inductor, it is necessary to calculate the snubber capacitors. Therefore, according to the next section, these capacitors are calculated, and finally, the inductor is calculated.

3.2 Design of Snubber Capacitors

In order to design snubber capacitors, reference [32] provides the complete design of these capacitors, which is generally provided for all converters.

$$i_{CS} = \frac{It}{t_f} \qquad 0 < t < t_f \tag{15}$$

$$V_{CS} = V_{DS} = \frac{1}{C_S}\int_0^t i_{CS}d_t = \frac{It^2}{2C_S t_f} \tag{16}$$

As a result,

$$C_S = \frac{I_{Lm}t_f}{2V_2} \tag{17}$$

Where t_f is the falling time of the switch current, I_{Lm} is the current of snubber capacitors in the converter, and V_2 is the voltage drop on the switch. t_f is the fall time of the switch, and by choosing the right switch, this value can be obtained from its datasheet page. Therefore, using this value and the current and voltage values in the converter, the snubber capacitors are calculated.

3.3 Voltage Gain in Boost Mode

To calculate voltage gain in boost mode, the voltage second balance of L_m is written.

$$\frac{V_1}{1+n}DT - \left(\frac{V_2 - V_1}{1+m}\right)(1-D)T = 0, \tag{18}$$

where T is period of switching, D is duty cycle, also n and m are ratio between L_1, L_2 and L_3, which are shown in below.

$$n = \frac{n_2}{n_1} \tag{19}$$

$$m = \frac{n_3}{n_1} \tag{20}$$

By simplifying Eq. (18), the voltage gain in boost mode is obtained as follows.

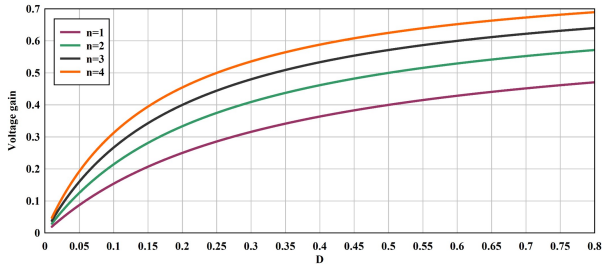

***Fig. 10**: Voltage gain in buck mode with various value of n.*

$$voltage\ gain = \frac{V_2}{V_1} = \frac{Dm - Dn + n + 1}{(1 - D)(1 + n)} \tag{21}$$

As Eq. (21) shows, coupled inductors have an effect on voltage gain, and with proper selection of n and m, high voltage gain can be obtained in the boost mode. To better understand these conditions, Figs. 8 and 9 are drawn, which show the voltage gain in boost mode with respect to n and m.

3.4 Voltage Gain in Buck Mode

Similar to the boost mode, in the buck mode the voltage gain is obtained by writing the voltage second balance on the L_m.

$$\left(V_2 - V_1\right) DT - \frac{V_1}{1 + n}(1 - D)T = 0 \tag{22}$$

As a result,

$$voltage\ gain = \frac{V_1}{V_2} = \frac{D(1 + n)}{2D + Dn + 1} \tag{23}$$

As the voltage gain relationship shows, in buck mode n has an effect on voltage gain. which, to better understand the graph in Fig. 10, is plotted.

As Figs. 8 and 9 show, m is very effective in generating voltage gain in boost mode, while n should be small in order to increase voltage gain in boost mode. In figure 10, it is clear that a low value of n is effective for lower voltage gain in buck mode, so these two values are selected for higher voltage gain in boost mode and lower voltage gain in buck mode. Also to compare voltage gain between converters, Fig. 11 is drawn, which shows the voltage gain in the proposed converter and other converters. As can be seen from this figure, the converters in [29] and [30] have a lower voltage gain than the proposed converter, but this voltage gain is fixed and is not controlled by any parameters except duty cycle. The voltage gain in the proposed converter can be changed by n.

3.5 Design and Select of Main Elements

The main elements of the proposed converter are selected or designed according to nominal power or voltage gain. Lm is the main inductor in the converter, which can be designed in a buck or boost configuration.

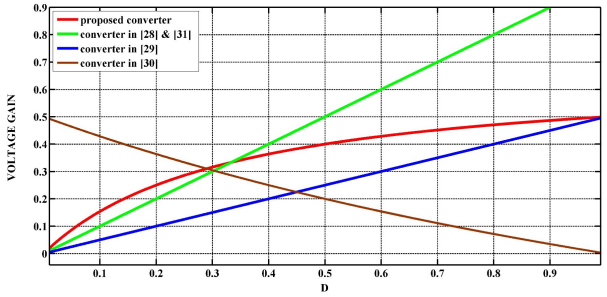

***Fig. 11**: Comparison between the proposed converter with other converters according to voltage gain in buck mode ($n = 1$).*

$$L_m = \frac{(1 - D)V_1}{\Delta_{ILm} f_{SW}}, \tag{24}$$

where Δ_{ILm} is the current ripple value on the inductor, which is usually considered 0.1 times the total current to ensure the work of the converter in CCM mode.

When the main inductor is designed, L_2 and L_3 are selected according to the voltage conversion ratio in the proposed converter. Therefore, the voltage gain equations and curves can be used to select n and m, then select L_2 and L_3 amounts.

To choose switches and diodes, it is considered what the current and voltage of these elements are. As a result, the element is used to withstand this current and voltage.

4. EXPERIMENTAL RESULTS

4.1 Results of Voltage and Current of Switches

A 300-W prototype of the proposed converter is implemented and tested to verify the theoretical analysis, which is shown in Fig. 12. Also, the specification of the proposed converter that is used to implement the converter is shown in Table 1.

The experimental results of the voltage and current

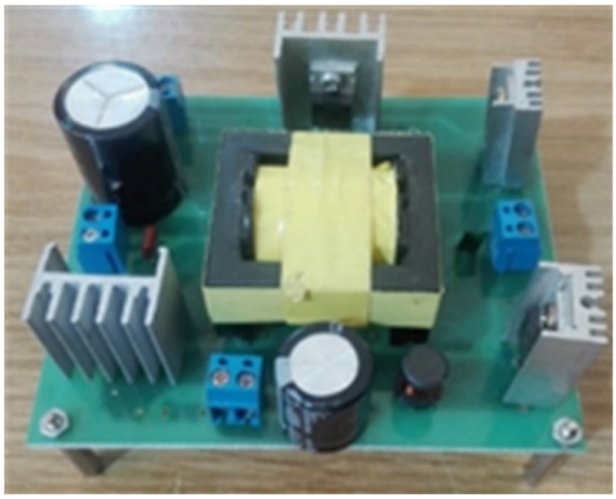

***Fig. 12**: Photograph of the proposed converter.*

***Table 1**: The proposed converter specification.*

Element	Value or Part number
S_1 and S_2	IRF740
D_1 and D_2	MUR1080
L_r	12μH
L_m	200μH
n	1
m	4
V_1	96 V
V_2	310 V
D	0.5
P	200 W
f_{SW}	100 kHz

of the semiconductor elements are presented in Figs. 13 (buck mode) and 14 (boost mode). In these figures, it is clear that the current of the switches is negative when the switches are turned on, which shows the ZVS condition is provided for these switches. The currents of D_1 and D_2 in these figures are changing slowly, which shows the ZCS condition is established for these diodes.

These figures compared to the theoretical figures show that the theoretical analysis of the converter is correct and that the shapes obtained in the experimental test are completely similar to the theoretical shapes. Only in some experimental results can small ripples be seen on the current or voltage, which are caused by the practical conditions of the test and the presence of coupled inductors, which create ripples on the elements at the moment of state change. On Figs. 13(b) and 14(b), the fluctuations in the switch voltage can be seen when changing the mode. These fluctuations are often caused by the presence of coupled inductors that are manually wound rather than industrially wound. Hence, these fluctuations can be reduced by winding the coupled inductors more precisely.

In order to prove the creation of ZVS conditions in different duty cycle ranges, Fig. 15 shows the voltage and current of converter switches in different duty cycles in buck and boost modes. As it is clear from this figure, in the duty cycle greater than or less than 0.5, soft switching conditions are available.

5. COMPARISON BETWEEN THE PROPOSED CONVERTER WITH OTHER CONVERTERS

5.1 Comparison Between the Proposed Converter with Conventional One

Due to the creation of a soft switching condition in the proposed converter and the reduction of losses in the elements, the converter efficiency is expected to increase. Therefore, the efficiency of the proposed converter is obtained for many values of the power and is drawn as a curve. This curve is shown in Figs. 16 and 17. In this figure, the efficiency of the conventional converter is also shown, which helps to compare the proposed converter

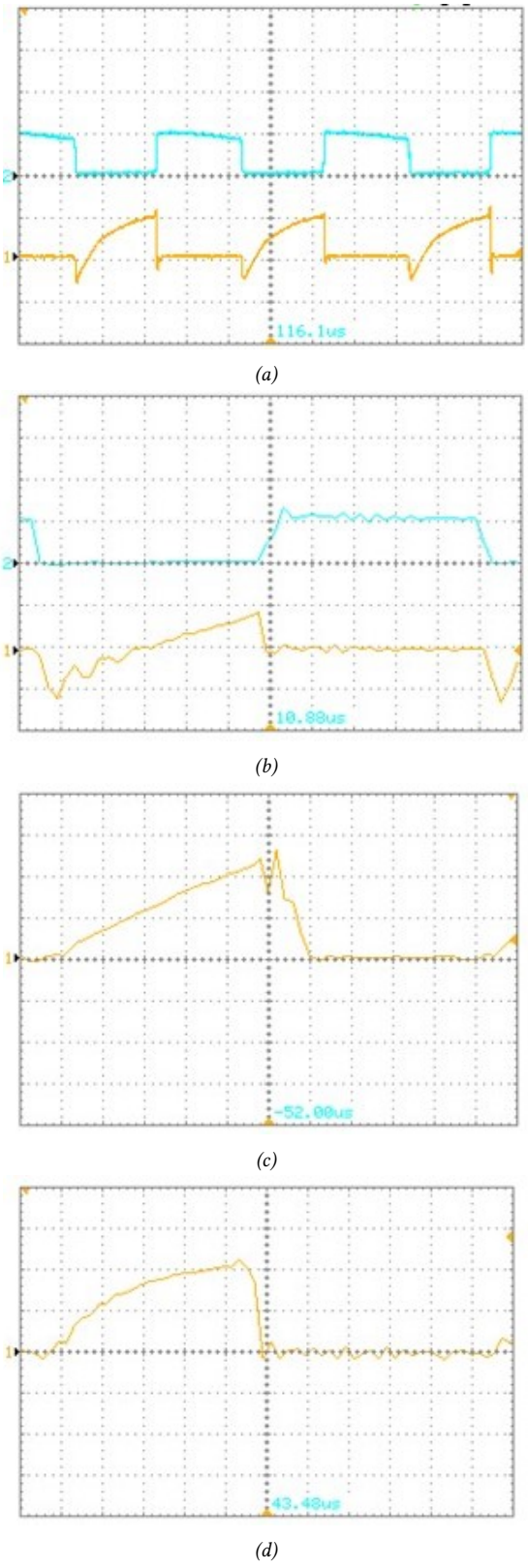

***Fig. 13**: The experimental results of the semiconductor devices in buck mode (a) Voltage (up) and current (down) of S_1 (300 volt/div or 1 A/div & 2.5 µs/div) (b) Voltage (up) and current (down) of S_2 (300 volt/div or 1 A/div & 1 µs/div) (c) Current of D_1 (0.5 A/div & 1 µs/div) (d) Current of D_2 (0.5 A/div & 1 µs/div).*

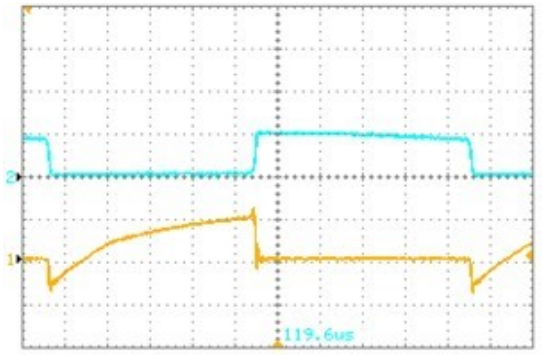

(a)

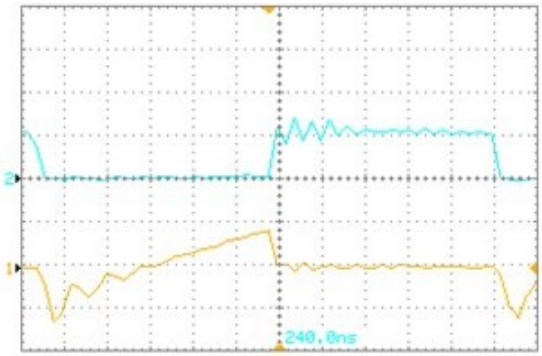

(b)

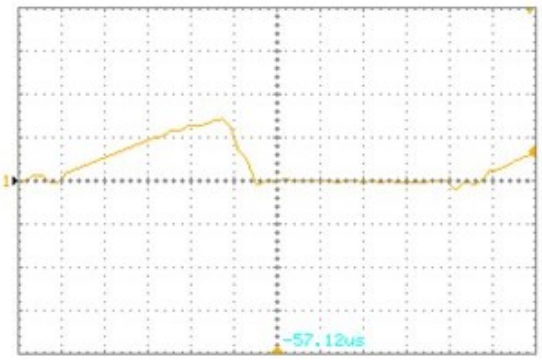

(c)

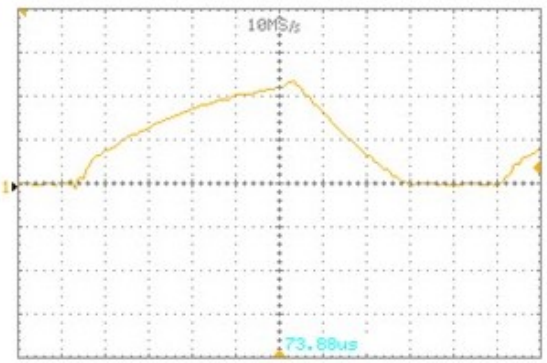

(d)

***Fig. 14**: The experimental results of the semiconductor devices in boost mode (a) Voltage (up) and current (down) of S_2 (300 volt/div or 1 A/div & 1 μs/div) (b) Voltage (up) and current (down) of S_1 (300 volt/div or 1 A/div & 1 μs/div) (c) Current of D_2 (1 A/div & 1 μs/div) (d) Current of D_1 (0.5 A/div & 1 μs/div).*

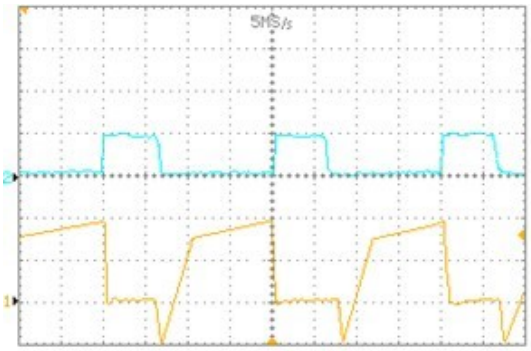

(a)

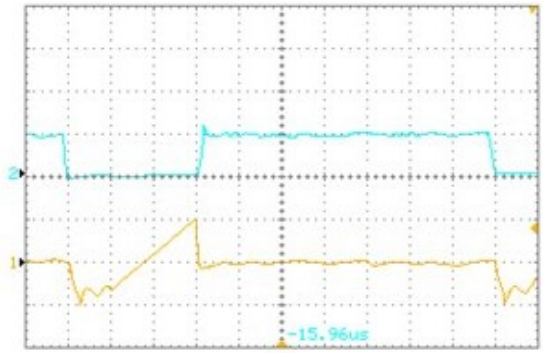

(b)

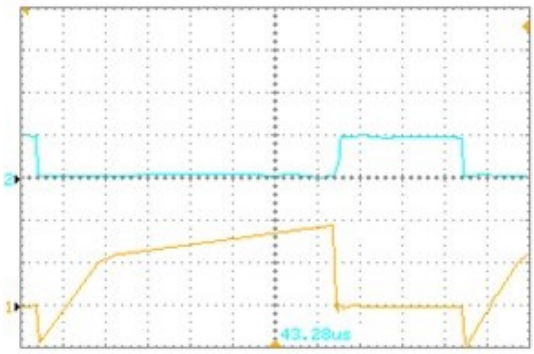

(c)

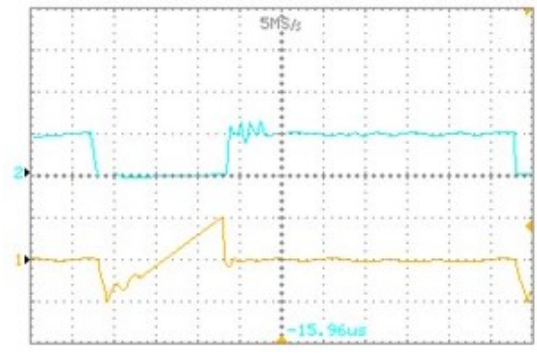

(d)

***Fig. 15**: The experimental results of the S_1 and S_2 in different value of duty cycle (D) in buck and boost mode (300 volt/div or 0.5 A/div &1 μs/div) (a) Voltage (up) and current (down) of S_1 in $D = 0.7$ and buck mode (b) Voltage (up) and current (down) of S_2 in $D = 0.3$ and buck mode (c) Voltage (up) and current (down) of S_2 in $D = 0.7$ and boost mode (d) Voltage (up) and current (down) of S_1 in $D = 0.3$ and boost mode.*

***Table 2**: Comparison between the proposed converter with four other soft switching converters.*

Converter / Parameters	[28]	[29]	[30]	[31]	Proposed
Number of Switches	8	4	3	8	2
Soft switching condition	ZVS	ZVS	ZCS	ZVS	ZVS
Efficiency	96.5%	95.5%	96%	95.5%	95.5%
Number of diodes	2	0	2	0	0
Number of coupled inductors	1	1	0	2	1
Voltage gain in boost mode	$\frac{n+2}{n(1-D)}$	$\frac{n+2}{(1-D)}$	$\frac{1+D}{1-D}$	$\frac{n+1}{(1-D)}$	$\frac{Dm-Dn+n+1}{(1-D)(1+n)}$
Voltage stress on switch	$\frac{V_{high}}{2}$	$\frac{V_{LOW}}{1-D}$	$\frac{V_1}{1-D}$	$\frac{V_{LOW}}{1-D}$	V_2
Current stress on switch	I_{Lm}	I_{in}	$I_{L1}+I_{L2}$	I_{in}	$\left(1+\frac{1}{n}\right)I_{Lm}$

***Table 3**: Comparison between the proposed converter with four other soft switching converters.*

Losses	Formula	Hard switching in boost mode	Hard switching in buck mode	Proposed converter in boost mode	Proposed converter in buck mode
Switching losses in S_1	$\left[\frac{1}{2}V_{DS1}I_{S1}\left(t_{on}+t_{off}\right)+V_{DS1}t_{rr}\left(I_{S1}+I_{rr}\right)\right]f_{SW}$	Zero	22.994W	Zero	Zero
Switching losses in S_2	$\left[\frac{1}{2}V_{DS2}I_{S2}\left(t_{on}+t_{off}\right)+V_{DS2}t_{rr}\left(I_{S2}+I_{rr}\right)\right]f_{SW}$	23.559W	Zero	Zero	Zero
Parasitic capacitance losses in S_1	$\frac{1}{2}C_{par}V_{DS1}^2f_{SW}$	N.A	2.63W	Zero	2.55W
Parasitic capacitance losses in S_2	$\frac{1}{2}C_{par}V_{DS2}^2f_{SW}$	2.51W	N.A	2.51W	Zero
Conduction losses in S_1	$I_{S1(rms)}^2R_{ds1}$	Zero	4.21W	0.4W	0.5W
Conduction losses in S_2	$I_{S2(rms)}^2R_{ds2}$	3.955W	Zero	0.45W	0.48W
Conduction losses in D_1	$V_{F(D1)}I_{F(D1-ave)}$	2.02W	2.02W	2.01W	2.02W
Conduction losses in D_2	$V_{F(D2)}I_{F(D2-ave)}$	1.87W	1.87W	1.78W	1.79W
Conduction loss in D_{S1}	$V_{F(DS1)}I_{F(DS1-ave)}$	0.4W	0.41W	0.35W	0.36W
Conduction loss in D_{S2}	$V_{F(DS2)}I_{F(DS2-ave)}$	0.34W	0.039W	0.3W	0.32W
Core loss of coupled inductors	$\frac{f_{SW}}{\frac{1\times10^9}{B^3}+\frac{1.1\times10^8}{B^{2.3}}+\frac{1.9\times10^6}{B^{1.65}}+1.9\times10^{-13}B^2f_{SW}^2}$	0.6W	0.6W	0.6W	0.6W
Conduction losses of L_1	$R_{L1}*I_{L1}^2$	0.065W	0.065W	0.065W	0.065W
Conduction losses of L_2	$R_{L2}*I_{L2}^2$	0.052W	0.052W	0.052W	0.052W
Conduction losses of L_3	$R_{L2}*I_{L2}^2$	0.075W	0.075W	0.075W	0.075W
Total losses	——	35.29W	35.546W	8.592W	8.912W

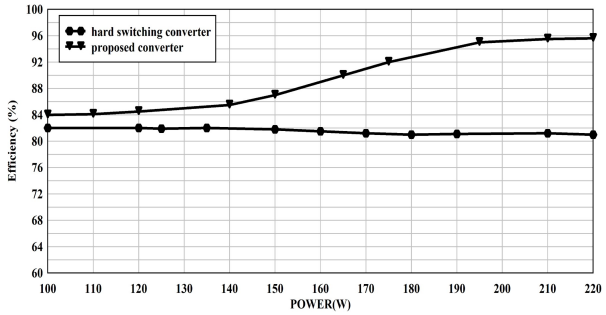

Fig. 16: Comparison between the proposed converter with hard switching converter in boost mode as efficiency.

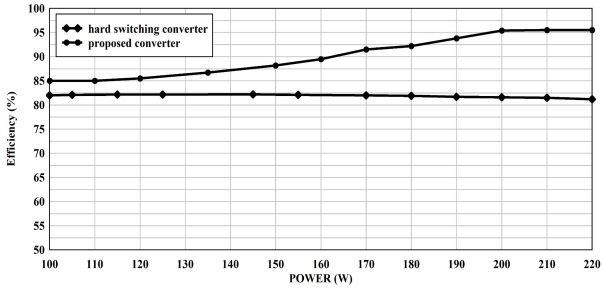

Fig. 17: Comparison between the proposed converter with hard switching converter in buck mode as efficiency.

with the conventional ones. As can be seen from this figure, the efficiency of the proposed converter is higher than that of conventional ones. Of course, as can be seen in the low power case, since the soft switching condition is not fully established, the efficiency of the proposed converter is low, but at the nominal power of the converter (300 W), the efficiency is high.

5.2 Comparison Between the Proposed Converter with Other Soft Switching Converters

The proposed converter is compared with four soft switching converters that have been introduced in recent years. The results of this comparison are presented in Table 2. In this table, as can be seen, the efficiencies are approximately the same. All four converters examined in this table have more switches than the proposed converter, which has increased the cost and volume of the converters. The converter in [28] has high efficiency but has eight switches with complex control on these switches. These conditions are present in [31]. Also in [31], there are two coupled inductors, which cause the volume and cost of this converter to increase. [30] has a fixed voltage gain, which is not parametrically controllable. It is true that the stress of the proposed converter is slightly higher than that of the other converters in the table, but the proposed converter has advantages such as a simple structure and simple control.

Table 3 shows the losses analysis of the proposed converter and the hard switching converter. These values show that the losses in the proposed converter are decreased and efficiency is increased.

6. CONCLUSION

In this paper, a new bidirectional converter with a simple structure is proposed. In the proposed converter without any auxiliary switch, a soft switching condition is established, which causes decreases in volume, cost, and losses in the converter. The control of the proposed converter is simple, and two switches are gated as complementary with each other, so it does not require any extra control circuitry. The proposed converter has three inductors that are wound on one core; hence, the volume of the converter is decreased. In the proposed converter, no additional stress is imposed on the semiconductor devices, so suitable semiconductor elements can be selected. Finally, the experimental results of the proposed converter verified the theoretical analysis.

REFERENCES

[1] N. Phankong and S. Chudjuarjeen, "A Photovoltaic Cell Energy Transfer System Using Series-Connected Bidirectional Resonant Converters," *ECTI Transactions on Electrical Engineering, Electronics, and Communications*, vol. 20, no. 1, pp. 114-122, Feb. 2022.

[2] R. Pandey and B. Singh, "Canonical Switching Cell (CSC) Converter-Based Power Factor-Corrected Battery Charger for E-Rickshaw," *IEEE Transactions on Industry Applications*, vol. 56, no. 5, pp. 5046-5055, May 2020.

[3] P. V. Mahesh, S. Meyyappan, and R. K. R. Alla, "A New Multivariate Linear Regression MPPT Algorithm for Solar PV System with Boost Converter," *ECTI Transactions on Electrical Engineering, Electronics, and Communications*, vol. 20, no. 2, pp. 269-281, Jun. 2022.

[4] R. Arulmurugan, "Photovoltaic powered transormerless hybrid converter with active filter for harmonic and reactive power compensation," *ECTI Transactions on Electrical Engineering, Electronics, and Communications*, vol. 16, no. 2, pp. 44-51, Feb. 2018.

[5] G. R. C. Mouli, J. Schijffelen, M. v. d. Heuvel, M. Kardolus, and P. Bauer, "A 10 kW Solar-Powered Bidirectional EV Charger Compatible With Chademo and COMBO," *IEEE Transactions on Power Electronics*, vol. 34, no. 2, pp. 1082-1098, Feb. 2019.

[6] A. Diab-Marzouk and O. Trescases, "SiC-Based Bidirectional Ćuk Converter with Differential Power Processing and MPPT for a Solar Powered Aircraft," *IEEE Transactions on Transportation Electrification*, vol. 1, no. 4, pp. 369-381, Dec. 2015.

[7] X. Zhang, C. Yin, and H. Bai, "Fixed-boundary-layer Sliding-mode and Variable Switching Frequency

Control for a Bidirectional DC–DC Converter in Hybrid Energy Storage System," *Electric Power Components and Systems*, vol. 45, no. 13, pp. 1474-1485, Aug. 2017.

[8] B. Wang, X. Zhang, U. Manandhar, H. B. Gooi, Y. Liu, and X. Tan, "Bidirectional Three-Level Cascaded Converter with Deadbeat Control for HESS in Solar-Assisted Electric Vehicles," *IEEE Transactions on Transportation Electrification*, vol. 5, no. 4, pp. 1190-1201, Sep. 2019.

[9] A. K. Singh, A. K. Mishra, K. K. Gupta, P. Bhatnagar, and T. Kim, "An Integrated Converter with Reduced Components for Electric Vehicles Utilizing Solar and Grid Power Sources," *IEEE Transactions on Transportation Electrification*, vol. 6, no. 2, pp. 439-452, Jun. 2020.

[10] V. Sohoni and Sh. Gupta, R. K. Nema, "Design of Wind-PV based Hybrid Standalone Energy Systems for Three Sites in Central India," *ECTI Transactions on Electrical Engineering, Electronics, and Communications*, vol. 17, no. 1, pp. 24-34, Sep. 2019.

[11] R. Rajasekaran and P. Usha Rani, "Bidirectional DC-DC converter for microgrid in energy management system," *international journal of electronics*, vol. 99, no. 8, pp. 1115-1131, 2012.

[12] X. Rong, J. K. H. Shek, and D. E. Macpherson, "The study of different unidirectional input parallel output series connected DC-DC converters for wind farm based multi-connected DC system," *International Transactions on Electrical Energy Systems*, vol. 31, no. 5, pp. 1-16, Mar. 2021.

[13] S. Punna, U. B. Manthati, and A. C. Raveendran, "Modeling, analysis, and design of novel control scheme for two-input bidirectional DC-DC converter for HESS in DC microgrid applications," *International Transactions on Electrical Energy Systems*, Jan. 2021.

[14] A. S. Samosir and A. H. M. Yatim, "Implementation of Dynamic Evolution Control of Bidirectional DC–DC Converter for Interfacing Ultracapacitor Energy Storage to Fuel-Cell System," *IEEE Transactions on Industrial Electronics*, vol. 57, no. 10, pp. 3468-3473, Oct. 2010.

[15] Z. Zhang, Z. Ouyang, O. C. Thomsen, and M. A. E. Andersen, "Analysis and Design of a Bidirectional Isolated DC–DC Converter for Fuel Cells and Supercapacitors Hybrid System," *IEEE Transactions on Power Electronics*, vol. 27, no. 2, pp. 848-859, Feb. 2012.

[16] H. Moradisizkoohi, N. Elsayad, and O. A. Mohammed, "A Family of Three-Port Three-Level Converter Based on Asymmetrical Bidirectional Half-Bridge Topology for Fuel Cell Electric Vehicle Applications," *IEEE Transactions on Power Electronics*, vol. 34, no. 12, pp. 11706-11724, Dec. 2019.

[17] S. M. P, M. Das, and V. Agarwal, "Design and Development of a Novel High Voltage Gain, High-Efficiency Bidirectional DC–DC Converter for Storage Interface," *IEEE Transactions on Industrial Electronics*, vol. 66, no. 6, pp. 4490-4501, Jun. 2019.

[18] W. Hassan, J. L. Soon, D. D.-C. Lu, and W. Xiao, "A High Conversion Ratio and High-Efficiency Bidirectional DC–DC Converter with Reduced Voltage Stress," *IEEE Transactions on Power Electronics*, vol. 35, no. 11, pp. 11827-11842, Nov. 2020.

[19] D. Yang, B. Duan, W. Ding, Ch. Zhang, J. Song, and H. Bai, "Turn-Off Delay-Controlled Bidirectional DC–DC Resonant Converter with Wide Gain Range and High Efficiency," *IEEE Transactions on Transportation Electrification*, vol. 6, no. 1, pp. 118-130, Mar. 2020.

[20] Y. Zhang, D. Zhang, J. Li, and H. Zhu, "Bidirectional LCLL Resonant Converter with Wide Output Voltage Range," *IEEE Transactions on Power Electronics*, vol. 35, no. 11, pp. 11813-11826, Nov. 2020.

[21] C. Bai, B. Han, B. H. Kwon, and M. Kim, "Highly Efficient Bidirectional Series-Resonant DC/DC Converter Over Wide Range of Battery Voltages," *IEEE Transactions on Power Electronics*, vol. 35, no. 4, pp. 3636-3650, Apr. 2020.

[22] J. Zeng, Z. Yan, J. Liu, and Z. Huang, "A High Voltage-Gain Bidirectional DC–DC Converter With Full-Range ZVS Using Decoupling Control Strategy," *IEEE Journal of Emerging and Selected Topics in Power Electronics*, vol. 8, no. 3, pp. 2775-2784, Sep. 2020.

[23] Z. Yan, J. Zeng, W. Lin, and J. Liu, "A Novel Interleaved Nonisolated Bidirectional DC–DC Converter with High Voltage-Gain and Full-Range ZVS," *IEEE Transactions on Power Electronics*, vol. 35, no. 7, pp. 7191-7203, Jul. 2020.

[24] R. H. Ashique and Z. Salam, "A High-Gain, High-Efficiency Nonisolated Bidirectional DC–DC Converter with Sustained ZVS Operation," *IEEE Transactions on Industrial Electronics*, vol. 65, no. 10, pp. 7829-7840, Oct. 2018.

[25] Y. -S. Lee, Y. -P. Ko, M. -W. Cheng, and L. -J. Liu, "Multiphase Zero-Current Switching Bidirectional Converters and Battery Energy Storage Application," *IEEE Transactions on Power Electronics*, vol. 28, no. 8, pp. 3806-3815, Aug. 2013.

[26] S. Rahimi, M. Rezvanyvardom, and A. Mirzaei, "A Fully Soft-Switched Bidirectional DC–DC Converter with Only One Auxiliary Switch," *IEEE Transactions on Industrial Electronics*, vol. 66, no. 8, pp. 5939-5947, Aug. 2019.

[27] R. H. Ashique and Z. Salam, "A Family of True Zero Voltage Zero Current Switching (ZVZCS) Nonisolated Bidirectional DC–DC Converter with Wide Soft Switching Range," *IEEE Transactions on Industrial Electronics*, vol. 64, no. 7, pp. 5416-5427, Jul. 2017.

[28] Z. Yan, J. Zeng, Z. Guo, R. Hu, and J. Liu, "A Soft-Switching Bidirectional DC–DC Converter With High Voltage Gain and Low Voltage Stress for Energy Storage Systems," *IEEE Transactions on*

Industrial Electronics, vol. 68, no. 8, pp. 6871-6880, Aug. 2021.

[29] R. Hu, J. Zeng, J. Liu, and K. W. Eric Cheng, "A Nonisolated Bidirectional DC–DC Converter With High Voltage Conversion Ratio Based on Coupled Inductor and Switched Capacitor," *IEEE Transactions on Industrial Electronics*, vol. 68, no. 2, pp. 1155-1165, Feb. 2021.

[30] M. P. Hirth, R. Gules, and C. H. I. Font, "A Wide Conversion Ratio Bidirectional Modified SEPIC Converter With Nondissipative Current Snubber," *IEEE Journal of Emerging and Selected Topics in Power Electronics*, vol. 9, no. 2, pp. 1350-1360, Apr. 2021.

[31] R. Hu, J. Zeng, Z. Yu, Z. Yan, and J. Liu, "Secondary Side Cascaded Winding-Coupled Bidirectional Converter with Wide ZVS Range and High Conversion Gain," *IEEE Journal of Emerging and Selected Topics in Power Electronics*, vol. 9, no. 2, pp. 1444-1454, Apr. 2021.

[32] N. Mohan, T. M. Undeland, and W. P. Robbins. *Power Electronics: Converters, Applications and Design*, 3rd ed. New York: Wiley, 2003.

Mahmood Vesali was born in Isfahan, Iran, in 1986. He received the B.S and M.S degrees in electrical engineering in 2008 and 2015 from Sepahan University and Islamic Azad University, khorasgan branch, respectively. He received the Ph.D degree also in electrical engineering in Islamic Azad University, khorasgan branch in 2020. His research interest are bidirectional DC-DC converters and soft switching DC-DC converters.

Marzieh Khorrami was born in Isfahan, Iran, in 1987. He received the B.S degrees in computer engineering in 2012 from Islamic Azad University, khorasgan branch (SAMA unit). Her research interest is on software, especially applied software in engineering.

Farhad Ghafoorian was born in Isfahan, Iran, in 1989. He received the B.S degrees in electrical engineering in 2013 from Islamic Azad University, Khomeini shahr branch. His research interest is switching power supply.